Modeling and Simulation for Dynamic Analysis of Column Type Electric Power Steering

T. TAMURA A. MAROONIAN M. HIGASHI R. FUCHS

A model is proposed for the analysis of the static and dynamic performance of a column type electric power steering (C-EPS) with relevant applications in system design and control. The basic inertia, stiffness and damping properties of each component are taken into consideration. Friction states in steering components change remarkably in normal operation conditions. Therefore a dynamic friction model (LuGre friction model) has been introduced for precise modeling of the losses in the gear meshes, the yoke support and the bearings. The torque ripple generated in the universal joints of the intermediate shaft is also taken into consideration. The assist motor (brushed DC type) and its power electronics are represented in a 4-quadrant model so as to represent power flow effect.

The developed model has been validated respectively for three subsystems (the assist motor, the power column and the rack & pinion). Finally, static and dynamic responses of this power steering model have been validated against experimental data of normal and inverse input.

***Key Words**: steering system, dynamic model, EPS, LuGre friction model*

1. Introduction

The operation of the steering system of a passenger car is characterized by frequent transitions from rest to turn. The steering velocity varies remarkably including the zero speed condition. Therefore, the friction of each component of the steering system often changes from the static to the dynamic state.

Friction affects the sensitivity characteristics of a steering actuator especially at the condition of relatively low driver input torque intended for small change of rack position. The friction reduction of the mechanical components of the steering is one of the countermeasures for this problem. Active friction compensation offers another option because the assist motor can generate a cancelling torque. In this case, a control law for the assist motor, which would alleviate the effect of friction, is designed based on a physical representation of the friction state.

The realization of these solutions requires a friction model, which represents the actual phenomena with minimum computational load, and a steering model for the prediction of the static and the dynamic characteristics.

Other published attempts in predicting power steering responses, for example[1, 2], apply more or less complex combinations of Maxwell and friction elements, which mathematical formulation is conditionally based. The computations of such models are known to be slow because of their discontinuous nature. A more accurate and computationally efficient representation of the friction is achieved with the LuGre model[3]. The LuGre model has been developed with the intention of representing accurately friction with a continuous state formulation and which could be used in control applications. Moreover, it gives a representation of the friction effects such as the Stribeck effect, stiction and hysteresis. To the best knowledge of the authors, only one work has been published on the application of the LuGre model to steering system[4].

The objective of this paper is to present the development of a model of the dynamics of a column assist electric power steering (C-EPS). The model is composed of inertia, stiffness, damping and friction elements. The computation of the actuator response should correlate with experimental measurements across the actual frequency range of operation. Typically, the response to a direct input, from driver to wheel, is defined within a bandwidth of about 5 Hz. A different bandwidth of about 30 Hz characterizes the response to an inverse input, from wheel to driver, so as to contain sufficient information for what is often refer to as "road feel".

* *This paper was prepared based on a report from the Society of Automotive Engineers of Japan. (Vol. 43, No. 2, March 2012, p.497-502).*

Three subsystem models (assist motor, column and rack-and-pinion) are developed and validated against experimental data. Finally, simulation results of direct inputs and inverse inputs typically used in the practice are compared against experimental data to confirm the adequacy of the proposed modeling approach.

2. Structure of the C-EPS

Figure 1 shows the structure of the steering actuator. This system is composed of

- a torsion bar used as a torque sensor for detecting the driver input torque,
- a DC motor and an ECU (electric control unit) for generating the assist torque corresponding to the driver torque,
- a worm gear for amplifying the motor torque,
- an intermediate shaft with two universal joints for transmitting the combined torque of the driver and the assist motor to the pinion gear and
- a rack and pinion gear for converting the motion from rotation to translation.

The parts located above the intermediate shaft form, what is called, the column. The performance of the steering system depends on the actuator layout. In this paper, a column assist electric power steering is considered.

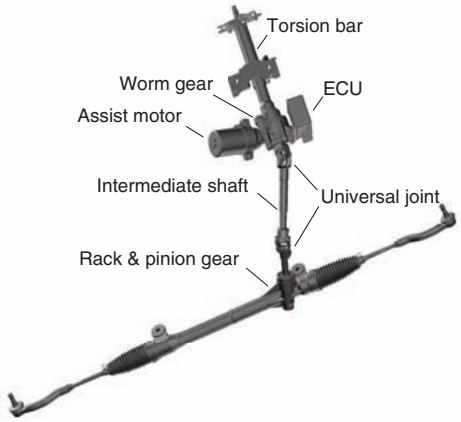

Fig. 1 Assembly view of JTEKT C-EPS

3. Modeling Assumptions and Approach

The proposed model assumes constant temperature and humidity conditions. The actuator is considered as an open-loop system composed of three IO ports: the driver port, the assist motor port and the rack port. When the torsion bar signal is fed back to the motor, the motor command depends on the driver input and the system is regarded as a two ports system.

The modeling approach consists in developing a model for each component of the steering such as the assist motor, the power column including the worm gear and the rack and pinion gear. Newton and Euler equations are applied for describing the motion of each inertia as a function of time. Furthermore, friction loss is considered at the gear meshing, the bearings and the rack guides (yoke support and bushes). The models are implemented in the MATLAB/Simulink environment.

4. Modeling

Figure 2 shows the 8-dof (degree-of-freedom) structure of the C-EPS model. The inputs and the outputs of the system are the steering wheel torque T_{sw}, the rack axial force F_{ld}, and the input torque signal E_{req}. In this figure, J and M represent the rotational inertias and the masses, ω and v the angular and the translational velocities, k and c the stiffness and the damping coefficients. The frictions at the mesh points of the worm gear and of the rack and pinion gear $F_{cf,ww}$, $F_{cf,wg}$, $F_{cf,p}$, $F_{cf,r}$ as well as that at these gear support bearings $T_{f,ww}$, $T_{f,wg}$, $T_{f,p}$ and at the rack guide $F_{f,gr}$ are considered. The suffix sw indicates the steering wheel, m the assist motor, ww the worm wheel, wg the worm gear, $u1$ and $u2$ the universal joints, p the pinion gear, r the rack gear, tb the torsion bar and int the intermediate shaft.

In the next section, the model is detailed along with experimental validation results for the friction, the assist motor, the power column and the rack and pinion gear subsystems.

4. 1 LuGre friction model

The friction generated in the transmission elements affects the steering performances. Therefore, physical modeling is required for predicting the effect of friction. Classical friction models, such as that of Coulomb, have discontinuous characteristics at zero slip (the relative velocity between the two surfaces) and therefore are not optimum for fast computation with numerical solvers. The LuGre friction model is based on a continuous state formulation and captures most of the observed effects. This model, developed from a joint research between the Lund Institute of Technology, Sweden and the University of Grenoble, France, is based on a representation of the average deflection force of elastic bristles (spring-like) at the friction interface. With this representation, it is only if the tangential forces to the contact surface are large enough that the bristle will slip. The friction coefficient is represented with a differential equation of the bristle deflection state. Moreover, this model captures typical friction effects such as the Stribeck effect, which occurs at the transition between mixed and hydrodynamic lubrication regimes. The friction coefficient decreases across that transition resulting in the stick–slip or stiction effect. Hence, the LuGre friction model enables fast

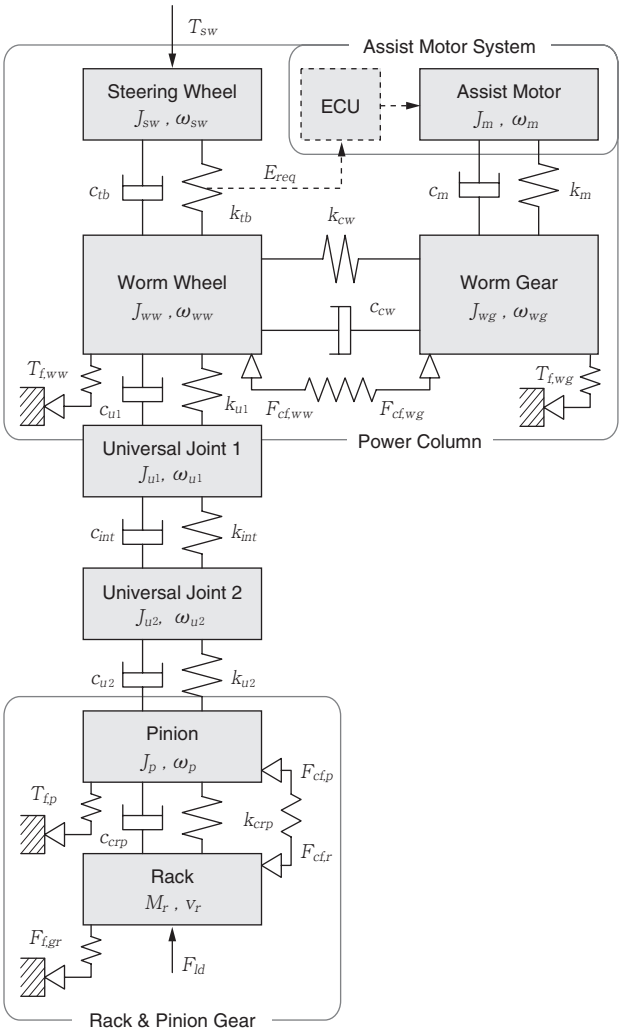

Fig. 2 Structure of C-EPS model

numerical computation and the application of model-based control theories because of its continuous and accurate nature.

The friction coefficient μ of the LuGre model is formulated as a function of the bristle deflection p and the slip v:

$$\mu = \sigma_0 p + \sigma_1 \dot{p} + \sigma_2 v \tag{1}$$

$$\dot{p} = v - \sigma_0 \frac{|v|}{g(v)} p \tag{2}$$

$$g(v) = \mu_c + (\mu_{ba} - \mu_c) e^{-(|v|/v_{sb})^2} \tag{3}$$

where μ_c is the Coulomb friction coefficient, μ_{ba} the peak friction coefficient, v_{sb} the Stribeck velocity, σ_0 and σ_1 the contact stiffness and damping coefficients in the tangential direction and σ_2 the viscous friction coefficient. Typically, these six parameters, related to the bristle state, are experimentally identified. The LuGre model is applied for representing the friction at the gear meshing, the bearings and the rack guides.

4. 2 Assist motor

Figure 3 shows a block diagram of the model of the assist motor and the ECU. The current target value E_{tgt}, which corresponds to the target torque of the motor, is calculated by the assist controller from the driver torque request E_{req} and the actual vehicle speed E_{veh}. Typically, the assist controller includes a map of the assist torque as a function of the driver torque request and the vehicle speed. Also, an instantaneous response of the torque sensor is assumed. The motion equation of the motor inertia J_m is described as follows:

$$J_m \dot{\omega}_m = T_m + T_{ml} \tag{4}$$

where T_m is the motor torque, defined as the product of the torque constant and the current i_m, and T_{ml} the motor load, represented by a stiffness and a damping elements (**Figure 2**). The current controller ensures high response and compensates the perturbation caused by the back electromotive force. The RL-circuit of the power

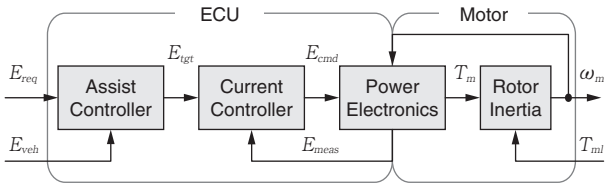

Fig. 3 Block diagram of ECU and assist motor model

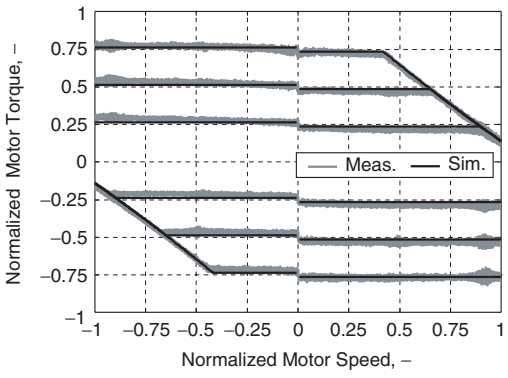

(a) Four-quadrant speed-torque characteristic

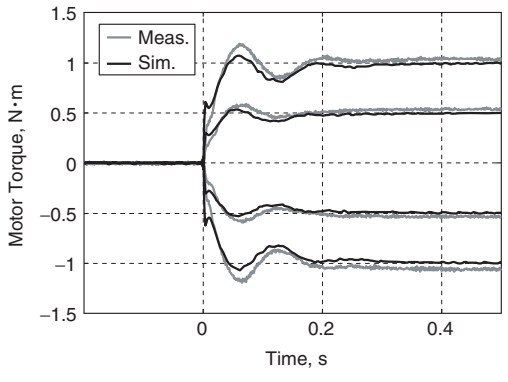

(b) ±0.5 N·m and ±1 N·m step responses

Fig. 4 Validation data for the model of the motor

electronics is represented as a linear system with the back electromotive force developed by the motor when rotating.

$$E_{cmd} = R_m i_m + L_m \dot{i}_m + k_{bef}\,\omega_m \tag{5}$$

where E_{cmd} is the command voltage, i_m the motor current, R_m and L_m the winding resistance and inductance and k_{bemf} the back electromotive force constant.

The saturation of the motor voltage is calculated from the battery voltage, the power consumption and the efficiency of the current driver circuit.

Figure 4 illustrates two comparisons between experimental measurements and simulation data of the assist motor. **Figure 4a** shows a normalized four quadrant graph of the speed and torque characteristic of the motor. In driving condition (first and third quadrants), the torque saturation at high speed, caused by the back electromotive force being not compensated by the current controller, is accurately reproduced. In the second and forth quadrants, when the motor is driven, constant torque is achieved independently of the speed. **Figure 4b** shows torque step responses when the motor shaft is fixed. Similar damping trend and good prediction accuracy are observed.

4. 3 Power column

The power column is composed of the assist motor, the torsion bar and the worm gear. The torque developed by the torsion bar T_{tb} is defined as follows:

$$T_{tb} = k_{tb}\int(\omega_{sw} - \omega_{ww})\,dt + c_{tb}\,(\omega_{sw} - \omega_{ww}) \tag{6}$$

The worm gear is represented with equivalent masses m_{wg}, m_{ww} concentrated at the pitch radius of the gear inertias J_{wg}, J_{ww}. **Figure 5** shows a planar view of the pitch circle around which the worm gear wrap. The worm gear friction depends on the normal force and the slip at the teeth contact. It is assumed that the motion of the worm gear and wheel are defined respectively along the x-axis and the y-axis only[5].

The gear meshing is represented by a single tooth with one or two contact points located on the pitch circle diameter. The pressure angle β_w, defined in the yz-plane, is assumed constant. The friction force is oriented at the lead angle γ_w, defined in the xy-plane. The worm gear motion equations write:

$$m_{wg}\dot{\vec{v}}_{wg} = \vec{F}_{wg,tot} + \vec{N}_{1,wg} + \vec{N}_{2,wg} + \vec{F}_{cf1,wg} + \vec{F}_{cf2,wg} \tag{7}$$

$$m_{ww}\dot{\vec{v}}_{ww} = \vec{F}_{ww,tot} + \vec{N}_{1,ww} + \vec{N}_{2,ww} + \vec{F}_{cf1,ww} + \vec{F}_{cf2,ww} \tag{8}$$

where v_{wg} and v_{ww} are the worm gear and the wheel velocities. These states are defined in their respective x and y directions and as a function of the pitch circle radius and angle. The total external force on the gear $F_{wg,tot}$, is the sum of the applied force F_{wg} and the support bearing frictions which depend on the radial forces $F_{br,wg}$ and $F_{ba,wg}$. The total force on the wheel $F_{ww,tot}$ is similarly defined. The normal force $N_{i,j}$ is defined from the teeth contact stiffness k_{cw} and damping c_{cw}:

$$N_{i,j} = k_{cw}\,(\Delta h_{i,cw} + h_{0,cw}) + c_{cw}\Delta\dot{h}_{i,cw} \tag{9}$$

$$i = 1, 2 \quad j = \ wg,\ ww$$

where the suffix i defines the upper and the lower contact point, $h_{0,cw}$ the initial deflection for the initial contact load and $\Delta h_{i,cw}$ the deflection variation. $\Delta h_{i,cw}$ is defined using x_{wg} and y_{ww} displacements, as follows:

$$\Delta h_{i,cw} = \pm\,(x_{wg}\sin(\gamma_w) - y_{ww}\cos(\gamma_w)) \quad i = 1, 2 \tag{10}$$

The tooth friction $F_{cfi,j}$ is a function of the slip v_{cw} dependent friction coefficient μ_{cw} and of the normal force N_{ij}:

$$F_{cfi,j} = \mu_{cw}(v_{cw})\ |N_{i,j}| \quad i = 1, 2 \quad j = \ wg,\ ww \tag{11}$$

$$\vec{v}_{cw} = \vec{v}_{wg} - \vec{v}_{ww} \tag{12}$$

The friction coefficient is obtained from the LuGre model presented in the relations (1) to (3). The six parameters of that model are experimentally identified. **Figure 6** shows a measurement example of the lumped friction coefficient of the complete worm gear module. This measurement was made with no load applied to the gear, enabling a direct estimation of the friction. Using

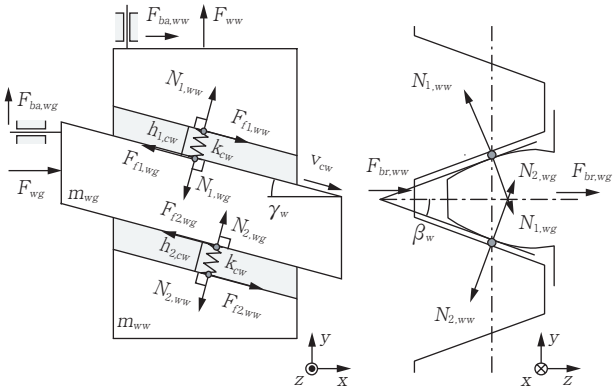

Fig. 5 Worm gear meshing

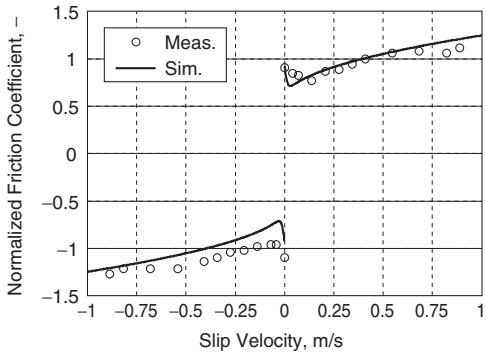

Fig. 6 Lumped friction characteristic of the power column

the power column with the assist motor, the friction torque was estimated by monitoring the current at a given velocity. Bearing losses being considerably smaller than the meshing friction, they can be neglected. Hence, only the meshing friction remains as shown in equations (7) and (8), and the parameters of the LuGre model can be estimated from the measured friction torque. The LuGre model of the worm gear mesh fitted to the experimental data is shown in **Figure 6**.

The model of the power column is validated with measured step responses and efficiency characteristics. **Figure 7** shows the measured and simulated efficiency characteristic of the worm gear. For this experiment, the worm gear is speed controlled (15 rpm at the worm wheel side) and a load torque is applied to the worm wheel. As shown, the model can predict the efficiency characteristics for both powerflow directions with the identified friction coefficient. The torque and speed conditions change frequently in normal driving situations. For example, when the worm gear torque is positive the assist motor power is also positive. Whereas, when the gear torque is negative, the assist motor is driven by the rack and pinion gear or the steering wheel, representing a negative power of the assist motor. Therefore, the representation of the gear efficiency in the two powerflow directions is required for an accurate prediction of the steering response.

Figure 8 shows three step responses from the three IO ports of the power column: the input shaft, the assist motor and the output shaft. This experiment was made by applying a torque step to a chosen input port, while the chosen output port was connected to a spring load. Good correlation between the measured and the simulated data is observed for the three step responses. In particular, the difference in the response damping for a torque step up and down is accurately replicated for the assist motor to output case.

4. 4 Intermediate shaft

The intermediate shaft is considered together with the two universal joints. The model represents the motion equations of the two universal joints coupled to the intermediate shaft. These equations are:

$$J_{u1}\dot{\omega}_{u1} = T_{u1} + T_{int}r_{u1} \tag{13}$$

$$J_{u2}\dot{\omega}_{u2} = T_{int} + T_{u2}r_{u2} \tag{14}$$

where r_{u1} and r_{u2} are the torque ratios representing the torque variation caused by the universal joints as a function of the rotating angle and the angle of orientation[6]. T_{u1} corresponds to the power column torque, T_{u2} the pinion gear torque and T_{int} the torque of the intermediate shaft. These three torques are defined with stiffness and damping elements as shown in **Figure 2**.

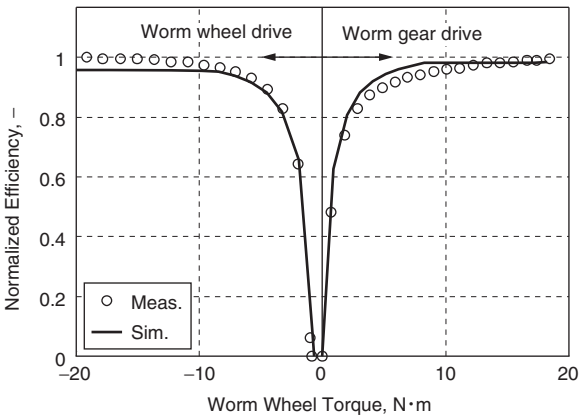

Fig. 7 Efficiency of the worm gear

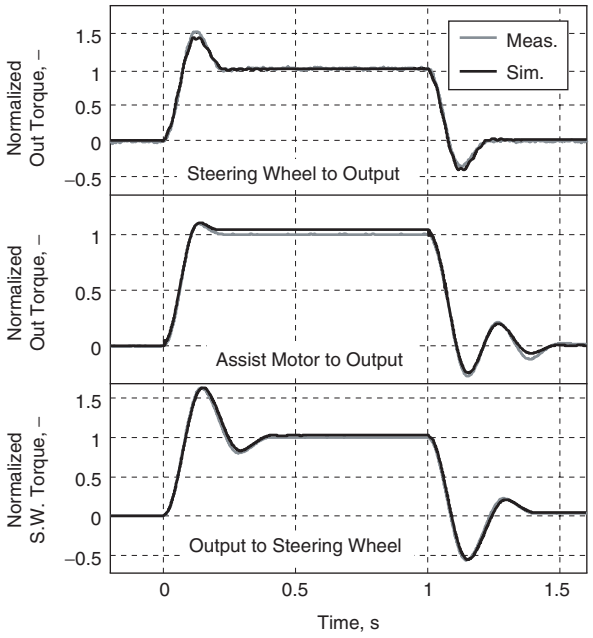

Fig. 8 Step responses of power column

4. 5 Rack and pinion gear

The rack and pinion gear converts the rotational motion of the column into the translational motion of the steering linkage on the chassis. A planar representation is used with equivalent masses m_p, m_r of the corresponding inertias as shown in **Figure 9**. The rack and pinion gear is modeled using the same assumptions and method as those made for the worm gear. Separate coordinates are defined with their respective suffixes p, r. It is assumed that the motion of the pinion and the rack gears are defined along their respective y-axis only. The motion equations are written as:

$$m_p\dot{\vec{v}}_p = \vec{F}_{p,tot} + \vec{N}_{1,p} + \vec{N}_{2,p} + \vec{F}_{cf\,1,p} + \vec{F}_{cf\,2,p} \tag{15}$$

$$m_r\dot{\vec{v}}_r = \vec{F}_{r,tot} + \vec{N}_{1,r} + \vec{N}_{2,r} + \vec{F}_{cf\,1,r} + \vec{F}_{cf\,2,r} \tag{16}$$

where v_p and v_r are the pinion and the rack gear velocities. The pinion axial displacement y_p is defined

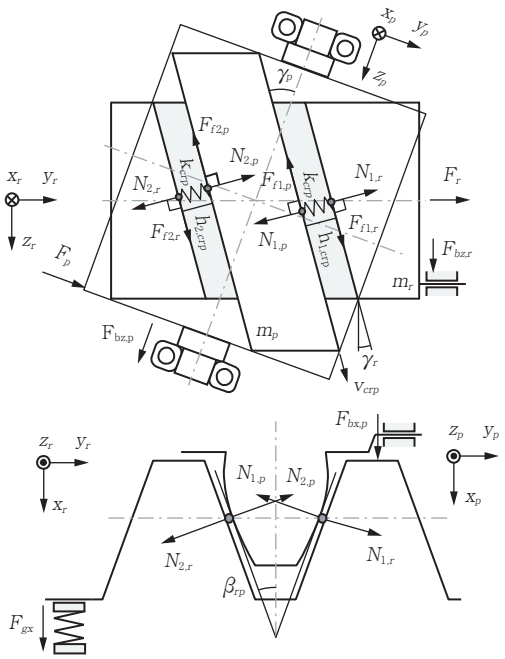

Fig. 9 Rack and pinion meshing

as a function of the pitch circle radius and angle. The total external force on the pinion $F_{p,tot}$, is the sum of the applied force F_p and the bearing frictions, which depend on the bearing force $F_{br,p}$ and the axial force $F_{bz,p}$. The total force on the rack $F_{r,tot}$ is defined similarly.

The friction coefficient of the mesh for the rack and pinion model was identified using the same methodology as that applied for the power column. **Figure 10** and **11** show the efficiency characteristic for both powerflow directions and the torque step responses from the two IO ports.

5. Simulation of the steering response

Simulations of the complete model are made under conditions similar to those met when testing actual steering systems in the practice. The parameters identified during the subsystems validation are kept constant. For this final validation, the torsion bar signal is fed back to the ECU input and the assist motor is controlled using the standard torque map of the assist controller (**Figure 3**).

The first validation is made with the steering torque versus angle characteristic. It corresponds to a standard test of direct input. For this experiment, the rack shaft was connected to a spring load. A sine waveform torque command of 0.5 Hz, 1 Hz, 1.5 Hz and 2 Hz was applied on the steering wheel and the corresponding angle was measured. **Figure 12** shows the comparison between the simulation results and the experimental measurements. For space and clarity reasons the test results up to 5Hz are not shown. The model reproduces accurately the torque versus angle characteristic of the actual steering

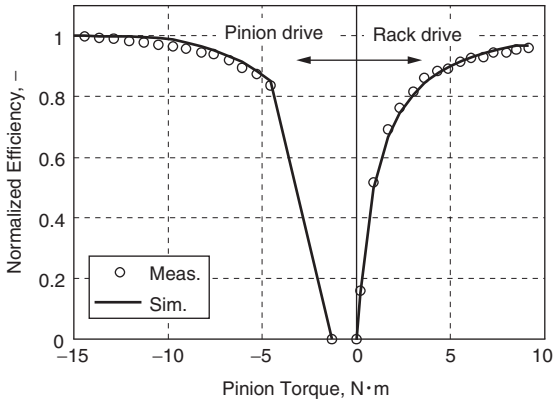

Fig. 10 Efficiency of rack and pinion gear

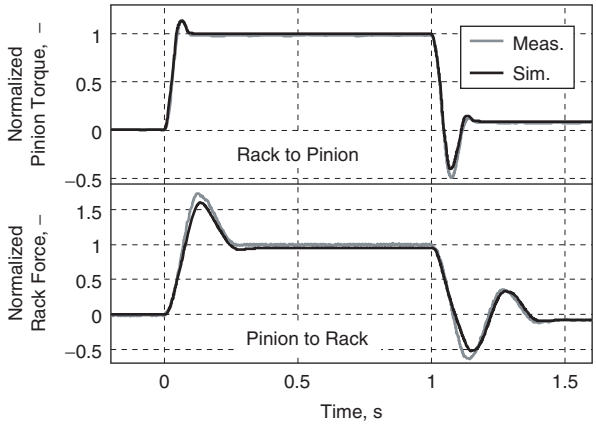

Fig. 11 Step responses of the rack and pinion gear

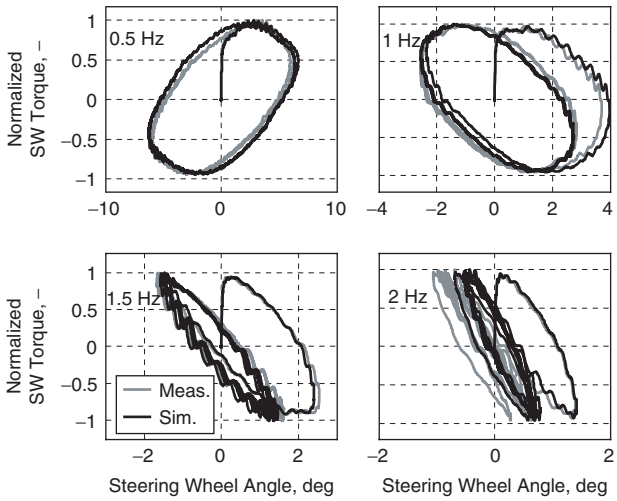

Fig. 12 Lissajous curves of the steering wheel angle to the steering wheel torque

within the frequencies bandwith of operation. The dead-band region where the torque rises from zero as well as the system hysteresis is predicted with the LuGre model representing both the static and the dynamic friction behaviors.

The rack force to steering wheel torque characteristic is

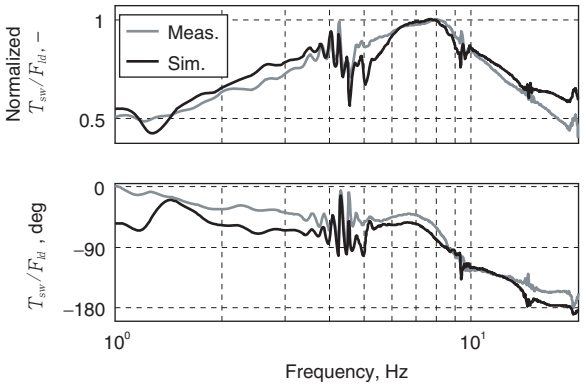

Fig. 13 Rack input response with steering wheel fixed

used as a second validation of the model. It corresponds to a standard test of inverse input. For this experiment, the steering wheel was fixed and a sine waveform force input was applied to one end of the rack bar by an external linear actuator (motor with ball screw). The frequency response of the system from 1 to 20 Hz was measured and is shown along with the simulation results in **Figure 13**. Adequate results are obtained with the simulation up to 15 Hz when comparing with the experimental data validating the proposed modeling approach.

The simulation results obtained match the experimental data of these standard tests with a relative error equal or smaller than 10%.

6. Conclusion

In order to deepen the understanding of the dynamics of the steering actuator, a model has been developed and experimentally validated. The particular characteristics of this C-EPS model are:

1. The representation of the friction transitions static to dynamic with the application of the LuGre model.
2. The replication of the efficiency in the two powerflow directions of the gear elements with a load dependent meshing friction model.
3. The prediction of the friction induced hysteresis of the standard steering torque versus angle characteristic.
4. A validated bandwidth of 5 Hz for a direct input and 15 Hz for an inverse input.

Further dynamic analysis of the steering actuator will be based on this model. The performance of the mechanical design can be optimized by identification of the dominant parameters. The development of a model-based control strategy taking advantage of the compatible friction representation could enable reduced and physically meaningful controller gain points improving the steering performance and simplifying the tuning work. On a higher level, this model could be used for analyzing the interaction with the vehicle for a better understanding of the overall steering performance.

References

1) Pfeffer, P.E. Harrer, M. Johnston, D.N. Shinde, R.P. : 2006. Modelling of a Hydraulic Steering System, F2006V164, FISITA (2006).
2) Ueda, E. Inoue, E. Sakai, Y. Hasegawa, M. Takai, H. Kimoto, S. : The Development of a Detailed Steering Model for On-Center Handling Simulation, AVEC (2002).
3) Canudas de Wit, C. Olsson, H. Åström, K. J. Lischinsky, P. : A New Model for Control of Systems with Friction, IEEE Transactions on Automatic Control, Vol. 40, No 3 (1995).
4) Pastorino, R. Naya, M.A. Pérez, J.A. Cuadrado, J : X-by-Wire Vehicle Prototype: A Steer-by-Wire System with Geared PM Coreless Motors, 7th Euromech Solid Mechanics Conference (2009).
5) Dohring, M.E. Lee, E. Newman, W.S. : A Load-Dependent Transmission Friction Model: Theory and Experiments, IEEE International Conference on Robotics and Automation (1993).
6) Seherr-Thoss, H. Chr. Schmelz, F. Aucktor, E. : Universal Joints and Driveshafts - Analysis, Design, Applications, Springer (2006).



T. TAMURA* A. MAROONIAN** M. HIGASHI**

R. FUCHS***

* *Mechanical Systems R&D Dept., Research & Development Headquarters*
** *Electronic Systems R&D Dept., Research & Development Headquarters*
*** *R&D Planning Dept., Research & Development Headquarters, Doctor of Mechatronics*